Volume 24, No 3 | International Journal of Radiation Research, July 2026

Hint1 mitigates high glucose- and radiation-induced apoptosis and inflammation in human retinal pigment epithelial cells through inhibiting the NF-κB pathway

W. Luo[1], R. Xu[2], P. Wu[1*], M. Yu[1], W. Dong[1]

[1]*Department of Ophthalmology, The Second Hospital & Clinical Medical School, Lanzhou University, Lanzhou, Gansu Province, China*
[2]*School of Public Health, Tianjin Medical University, Tianjin, China*

► ***Original article***

Corresponding author:
Pengcheng Wu, M.D.,
E-mail: *wupch@lzu.edu.cn*

Received: May 2026
Final revised: June 2026
Accepted: July 2026

Int. J. Radiat. Res., July 2026; 24(3): 819-829

DOI: 10.61186/ijrr.24.3.32

Keywords: *Histidine triad nucleotide-binding protein 1, diabetic retinopathy, retinal pigment epithelium, radiation injuries, apoptosis*

ABSTRACT

Background: Histidine triad nucleotide-binding protein 1 (Hint1) has been associated with inflammation, apoptosis, and the DNA damage response. However, its potential role in RPE injury induced by high glucose and/or radiation is unclear. We evaluated the protective effects of Hint1 against high-glucose and irradiation-induced RPE cell injury and the underlying mechanism involved the NF-κB pathway. ***Materials and Methods:*** The expression of Hint1 was determined in retinas from mice with type 1 diabetes and in human RPE cells with high-glucose and/or irradiation injury. Modulation of Hint1 protein levels was achieved through Hint1-overexpression and knockdown. Cellular apoptosis, DNA damage, cytokine production, and NF-κB activity were measured by flow cytometry, γH2AX immunofluorescence/Western blot, real-time PCR, ELISA, Western blot, and p65 translocation assay. BAY 11-7082 was used for mechanism validation. ***Result:*** Expression of Hint1 was down-regulated in diabetic retinal tissues and in ARPE-19 cells under combined exposure to hyperglycemia and radiation conditions with the most severe downregulation seen in the case of combined stimuli. The combination increased apoptosis, γ-H2AX levels, TNF-α, IL-6, and IL-8 expression, and nuclear translocation of phosphorylated p65. Overexpression of Hint1 reduced apoptosis, DNA damage, and cytokine release, whereas knockdown of Hint1 increased them. Inhibition of NF-κB partially reversed the detrimental effects of Hint1 deficiency. ***Conclusion:*** Hint1 attenuates high-glucose- and radiation-induced RPE cell injury, particularly under combined stress, at least in part by suppressing NF-κB activation. These findings suggest that the Hint1/NF-κB axis may represent a potential therapeutic target for retinal injury associated with diabetes and radiotherapy.

INTRODUCTION

Diabetic retinopathy (DR) is one of the most common microvascular complications of diabetes mellitus and has become a leading cause of adult blindness worldwide [1, 2]. Inflammatory and adhesion -related pathways have also been implicated in diabetes susceptibility and vascular complications [3, 4]. Its pathological progression primarily involves increased retinal vascular permeability, microvascular occlusion, and neovascularization [5, 6]. Retinal pigment epithelial (RPE) cells, as a core component of the outer blood-retinal barrier, play a critical role in maintaining the structural stability and functional integrity of the retina [7, 8]. Previous studies have demonstrated that high glucose-induced oxidative stress, inflammatory responses, and apoptosis are key mechanisms contributing to RPE dysfunction [9,10].

Radiation retinopathy represents another significant cause of retinal injury, occurring in patients receiving radiotherapy for ocular, orbital, or head and neck malignancies [11, 13]. The pathological features of radiation retinopathy - including vascular endothelial damage, capillary occlusion, inflammation, and RPE degeneration - closely parallel those observed in diabetic retinopathy [14, 15]. Ionizing radiation directly induces DNA double-strand breaks, generates reactive oxygen species (ROS), and activates pro-inflammatory signaling cascades, particularly the NF-κB pathway [16, 18]. Notably, patients with diabetes who undergo radiation therapy may experience accelerated and more severe retinal damage, suggesting a potential synergistic effect between hyperglycemia and radiation-induced stress [19, 20]. However, the molecular mechanisms underlying this interaction in RPE cells remain poorly characterized.

Histidine triad nucleotide-binding protein 1 (Hint1) is a ubiquitously expressed nucleocytoplasmic protein belonging to the HINT family. It exerts multiple biological functions, including participation in signal transduction, DNA repair, and transcriptional regulation [21, 22]. Several

studies have shown that Hint1 can inhibit inflammation, apoptosis, and tumor progression in cancers and metabolic disorders [23, 24]. Recent evidence also suggests that Hint1 may be involved in cellular responses to genotoxic stress and DNA damage repair [25]. However, its potential protective role in diabetic ocular diseases and radiation-induced retinal injury remains unclear, particularly in the context of RPE cell injury under combined metabolic and genotoxic stress.

The NF-κB signaling pathway is a central regulator of cellular stress responses and plays a pivotal role in the development of both diabetic and radiation retinopathies. A high-glucose environment or ionizing radiation exposure can independently activate the NF-κB pathway, which in turn promotes the release of pro-inflammatory cytokines and triggers apoptosis [26-28]. Given the central role of NF-κB in integrating various stress signals, investigating the regulatory relationship between Hint1 and the NF-κB signaling pathway under combined hyperglycemic and radiation stress may reveal new therapeutic opportunities for retinal protection.

The current study sought to determine whether Hint1 is involved in apoptosis, inflammation, DNA damage, and NF-κB signaling pathways following exposure to hyperglycemia, irradiation, and their combined effect in ARPE-19 cells. The uniqueness of the current study lies in the analysis of Hint1 in the context of hyperglycemia and irradiation-induced injury of retinal pigment epithelium cells, which is a reality in the clinic but an under researched topic, especially among diabetic patients who have to undergo radiation therapy. In addition, Hint1 overexpression, Hint1 downregulation, and pharmacological inhibition of signaling were employed in this study to understand the mechanism of Hint1/NF-κB signaling pathway interaction, which may serve as a natural protective mechanism against metabolic and genotoxic stress in RPE cells.

MATERIALS AND METHODS

Experimental animals

Eight-week-old male C57BL/6 mice were purchased from Kennan Biotechnology Co., Ltd. and were randomly divided into three groups: a normal control group, a streptozotocin (STZ)-induced diabetes mellitus without retinopathy (STZ without retinopathy) group, and an STZ-induced diabetes mellitus with retinopathy (STZ with retinopathy) group, with eight mice in each group. Diabetes was induced by intraperitoneal injection of STZ (50 mg/kg body weight; Sigma-Aldrich, St. Louis, MO, USA; Cat. No. S0130) dissolved in sodium citrate buffer (pH 4.5) for five consecutive days. Control mice received citrate buffer only. Blood glucose levels were measured 72 hours after the final injection, and mice with blood glucose levels > 16.7 mmol/L were considered diabetic. Mice were maintained for 12 weeks post-induction to allow development of retinal complications. Before the start of the experiment, the mice were housed in an environment maintained at 22 ± 2°C with 55% ± 10% relative humidity and a 12-hour light/dark cycle with free access to food and water. At the end of the experiment, mice were euthanized by cervical dislocation under deep anesthesia, and their eyeballs were collected for the detection of Hint1 protein and mRNA expression levels.

Cell culture and treatment

Human retinal pigment epithelial cells ARPE-19 cells (CRL-2302; American Type Culture Collection, Manassas, VA, USA) were purchased from the American Type Culture Collection (ATCC, Manassas, VA, USA). Cells were cultured in DMEM/F12 medium (Gibco, Grand Island, NY, USA) supplemented with 10% fetal bovine serum (FBS; Gibco, Grand Island, NY, USA; Cat. No. 10099-141) and 1% penicillin-streptomycin (Gibco, Grand Island, NY, USA; Cat. No. 15140-122) in a humidified incubator at 37°C with 5% CO_2. A high-glucose injury model was established by treating the cells with 30 mmol/L D-glucose (Sigma-Aldrich, St. Louis, MO, USA; Cat. No. G8270) for 24 hours. For osmotic control, cells were treated with 30 mmol/L mannitol (sigma-Aldrich, St. Louis, MO, USA; Cat. No. M4125) in parallel experiments.

Radiation exposure

ARPE-19 cells were seeded in 6-well plates and cultured to 70–80% confluency prior to irradiation. Cells were irradiated at room temperature using an X-ray biological irradiator (X-RAD 225, Precision X-Ray Inc., North Branford, CT, USA) operating at 225 kVp and 13.3 mA, with a 0.3 mm copper filter, at a dose rate of 2.5 Gy/min. The following radiation doses were tested in preliminary dose-response experiments: 0, 2, 5, and 10 Gy. Based on preliminary dose-response experiments evaluating apoptosis and Hint1 expression, 5 Gy was selected for subsequent experiments. For combined treatment groups, cells were first exposed to high glucose (30 mmol/L) for 12 hours, followed by 5 Gy irradiation, and then incubated for an additional 24 hours before downstream analyses. Sham-irradiated controls were handled identically but without radiation delivery. The experimental treatment groups are summarized in table 1.

Table 1. Experimental treatment groups used in the in vitro ARPE-19 cell injury model.

Group	Glucose Concentration	Radiation Dose
Control	5.5 mmol/L	Sham (0 Gy)
HG	30 mmol/L	Sham (0 Gy)
IR	5.5 mmol/L	5 Gy
HG + IR	30 mmol/L	5 Gy

Abbreviations: Hint1, histidine triad nucleotide-binding protein 1; TNF-α, tumor necrosis factor-alpha; IL-6, interleukin-6; IL-8, interleukin-8; GAPDH, glyceraldehyde-3-phosphate dehydrogenase; bp, base pairs.

Cell transfection

The Hint1 overexpression plasmid (pcDNA3.1-Hint1) and small interfering RNA targeting Hint1 (si-Hint1) were synthesized by Shanghai Gemma Biotechnology Co., Ltd (Shanghai, China). The si-Hint1 target sequence was 5′-GCAAGAUCUUCUUCAACUATT-3′ (sense) and 5′-UAGUUGAAGAAGAUCUUGCTT-3′ (antisense). An empty vector (pcDNA3.1) and negative control siRNA (si-NC; 5′-UUCUCCGAACGUGUCACGUTT-3′) were used as controls. Transfections were performed using Lipofectamine™ 3000 reagent (Invitrogen, Carlsbad, CA, USA; Cat. No. L3000015) according to the manufacturer's instructions. Cells were transfected at 50%–70% confluency with 2.5 μg plasmid DNA or 50 nM siRNA, followed by the indicated glucose and radiation treatments. Cells were harvested 48 hours after transfection for subsequent analyses.

Reverse transcription quantitative polymerase chain reaction (RT-qPCR)

Total RNA from ARPE-19 cells and mouse retinal tissues was extracted using TRIzol™ reagent (Thermo Fisher Scientific, Waltham, MA, USA; Cat. No. 15596026). RNA concentration and purity were assessed using a NanoDrop 2000 spectrophotometer (Thermo Fisher Scientific, Waltham, MA, USA), with A260/A280 ratios between 1.8 and 2.0 considered acceptable. One microgram of total RNA was reverse-transcribed into cDNA using the PrimeScript™. RT Master Mix Kit (TaKaRa Bio Inc., Shiga, Japan; Cat. No. RR036A) according to the manufacturer's protocol. RT-qPCR was performed on an ABI Prism 7500 Real-Time PCR System (Applied Biosystems) using SYBR® Premix Ex Taq™ II (TaKaRa Bio Inc., Shiga, Japan; Cat. No. RR420A). Amplification was performed under standard cycling conditions, and melt curve analysis was used to confirm amplification specificity. Each sample was analyzed in triplicate. Relative gene expression was calculated using the $2^{-\Delta\Delta Ct}$ method, with GAPDH as the internal reference gene. Relative gene expression levels were calculated using the $2^{-\Delta\Delta Ct}$ method, with GAPDH serving as the internal reference gene. The primer sequences used in this study are listed in table 2.

Western blotting

Total protein was extracted from ARPE-19 cells and mouse retinal tissues using RIPA lysis buffer (Beyotime Biotechnology, Shanghai, China; Cat. No. P0013B) supplemented with 1 mmol/L phenylmethylsulfonyl fluoride (PMSF; Beyotime Biotechnology, Shanghai, China; Cat. No. ST506), protease inhibitor cocktail (Roche, Basel, Switzerland; Cat. No. 04693159001), and phosphatase inhibitor cocktail (Roche, Basel, Switzerland; Cat. No. 4906845001). Nuclear and cytoplasmic proteins were isolated using the NE-PER™ Nuclear and Cytoplasmic Extraction Kit (Thermo Fisher Scientific, Waltham, MA, USA; Cat. No. 78833) according to the manufacturer's instructions. Protein concentrations were determined using a bicinchoninic acid (BCA) Protein Assay Kit (Beyotime Biotechnology, Shanghai, China; Cat. No. P0010S), and equal amounts of protein (20 μg per lane) were separated by 10% or 12% SDS-PAGE and transferred onto polyvinylidene difluoride (PVDF) membranes (MilliporeSigma, Burlington, MA, USA; Cat. No. IPVH00010).

Table 2. Primers used for RT-qPCR.

Gene	Forward primer (5′–3′)	Reverse primer (5′–3′)	Product size (bp)
Hint1 (human)	GAGATGG-CAGATGAGATT	TTAACCAGGA GGCCAATG	384*
Hint1 (mouse)	GAGATGG-CAGACGAGATC	TTAACCAGGA GGCGAATG	384*
TNF-α	ATGAGCACTGA AAGCATGATC	TCACAGGGCAATGATCC CAAAGTAGACCTGCCC	702
IL-6	ATGAACTCCT TCTCCACAAGC	CTACATTTGCCGAAGAG CCCTCAGGCTGGACTG	639
IL-8	ATGACTTCCAA-GCTGGCCGTG	TTATGAATTCTCAGCC CTCTTCAAAAACTTCTC	300–302*
GAPDH (human)**	GCGGGAAATCG TGCGTGACATT	GATGGAGTTGAAGG TAGTTTCGTG	232**
GAPDH (mouse)	AGGTCGGTGT GAACGGATTTG	TGTAGACCATGTAG TTGAGGTCA	123

Data are presented as mean ± standard deviation (SD) percentage reduction compared with the respective vector control group. *P < 0.05 versus the percentage reduction in the high-glucose (HG) group, analyzed by one-way analysis of variance (ANOVA) followed by Tukey's post hoc test. Abbreviations: Hint1, histidine triad nucleotide-binding protein 1; HG, high glucose; IR, ionizing radiation; HG + IR, combined high glucose and ionizing radiation; TNF-α, tumor necrosis factor-alpha; IL-6, interleukin-6; IL-8, interleukin-8; NF-κB, nuclear factor-kappa B; p-p65, phosphorylated p65; SD, standard deviation; ANOVA, analysis of variance.

After blocking with 5% non-fat milk in TBST for 2 hours at room temperature, membranes were incubated overnight at 4°C with the following primary antibodies: anti-Hint1 (1:1000; Abcam, Cambridge, UK; Cat. No. ab124879), anti-cleaved caspase-3 (Asp175; 1:1000; Cell Signaling Technology, Danvers, MA, USA; Cat. No. 9664), anti-Bcl-2 (1:2000; Abcam, Cambridge, UK; Cat. No. ab196495), anti-phospho-NF-κB p65 (Ser536; 1:1000; Cell Signaling Technology, Danvers, MA, USA; Cat. No. 3033), anti-NF-κB p65 (1:1000; Cell Signaling Technology, Danvers, MA, USA; Cat. No. 8242), anti-γ-H2AX (Ser139; 1:1000; Cell Signaling Technology, Danvers, MA, USA; Cat. No. 9718), anti-Lamin B1 (1:2000; Abcam, Cambridge, UK; Cat. No. ab16048), and anti-GAPDH (1:2000; Abcam, Cambridge, UK; Cat. No. ab9485). Membranes were then incubated with horseradish peroxidase-conjugated secondary antibodies (goat anti-rabbit IgG H&L, 1:5000; Abcam, Cambridge, UK; Cat. No. ab205718; goat anti-mouse IgG H&L, 1:5000; Abcam, Cambridge, UK; Cat. No. ab205719) for 2 hours at room temperature.

Protein bands were visualized using enhanced chemiluminescence reagent (Thermo Fisher Scientific, Waltham, MA, USA; Cat. No. 34095), and images were captured using a ChemiDoc XRS+ gel imaging system (Bio-Rad Laboratories, Hercules, CA, USA). Band intensities were quantified using ImageJ

software, version 1.53 (National Institutes of Health, Bethesda, MD, USA), and normalized to GAPDH for total/cytoplasmic proteins or Lamin B1 for nuclear proteins.

Enzyme-linked immunosorbent assay (ELISA)

The concentrations of TNF-α, IL-6, and IL-8 in cell culture supernatants were measured using commercial ELISA kits according to the manufacturers' instructions: Human TNF-α ELISA Kit (Invitrogen, Cat. No. KMC1011; detection range: 7.8–500 pg/mL), Human IL-6 ELISA Kit (Invitrogen, Cat. No. KMC0061; detection range: 3.1–200 pg/mL), and Human IL-8 ELISA Kit (Thermo Fisher Scientific, Cat. No. 88-8086-22; detection range: 3.9-250 pg/mL). Absorbance was measured at 450 nm with wavelength correction at 570 nm using a SpectraMax i3x microplate reader (Molecular Devices). Cytokine concentrations were calculated from four-parameter logistic standard curves.

Flow cytometric analysis of apoptosis

Apoptosis levels were assessed using the FITC Annexin V Apoptosis Detection Kit I (BD Biosciences, Cat. No. 556547). Cells (including floating cells in the culture supernatant) were collected, washed twice with cold PBS, and resuspended in 1× binding buffer at a concentration of 1×10^6 cells/mL. A 100 μL aliquot of the cell suspension was incubated with 5 μL of Annexin V-FITC and 5 μL of propidium iodide (PI) for 15 minutes at room temperature in the dark. After incubation, 400 μL of 1× binding buffer was added, the samples were gently mixed, and immediately analyzed using a FACSCalibur flow cytometer (BD Biosciences, USA) equipped with a 488 nm argon laser. For each sample, at least 10,000 events were acquired. Data were analyzed using FlowJo software (version 10.8, Tree Star Inc.). Apoptotic and necrotic cell populations were identified as follows: viable cells (Annexin V^-/PI^-), early apoptotic cells (Annexin V^+/PI^-), late apoptotic cells (Annexin V^+/PI^+), and necrotic cells (Annexin V^-/PI^+). Total apoptosis was defined as the sum of early and late apoptotic populations.

Immunofluorescence staining

Immunofluorescence staining was performed to evaluate NF-κB p65 phosphorylation/nuclear translocation and γ-H2AX foci formation. ARPE-19 cells grown on coverslips were fixed with 4% paraformaldehyde (Sigma-Aldrich, St. Louis, MO, USA; Cat. No. 30525), permeabilized with 0.2% Triton X-100 (Sigma-Aldrich, St. Louis, MO, USA; Cat. No. T8787), blocked with 5% bovine serum albumin (BSA; Sigma-Aldrich, St. Louis, MO, USA; Cat. No. A7906), and incubated overnight at 4°C with rabbit anti-phospho-NF-κB p65 (Ser536; 1:250; Cell Signaling Technology, Danvers, MA, USA; Cat. No. 3033S) or mouse anti-γ-H2AX (Ser139; 1:200; MilliporeSigma, Burlington, MA, USA; Cat. No. 05-636). Cells were then incubated with Alexa Fluor 488-conjugated goat anti-rabbit IgG (1:500; Invitrogen, Carlsbad, CA, USA; Cat. No. A11001) or Alexa Fluor 594-conjugated goat anti-mouse IgG (1:500; Invitrogen, Carlsbad, CA, USA; Cat. No. A11005) secondary antibodies and counterstained with DAPI (Beyotime Biotechnology, Shanghai, China; Cat. No. C1002). Coverslips were mounted using ProLong™ Gold Antifade Mountant (Invitrogen, Carlsbad, CA, USA; Cat. No. P36930).

Images were acquired using a Leica DMI3000B fluorescence microscope or a Leica TCS SP8 confocal laser scanning microscope (Leica Microsystems, Wetzlar, Germany) under identical acquisition settings across groups. Nuclear co-localization of p-NF-κB p65 was quantified using ImageJ software, version 1.53 (National Institutes of Health, Bethesda, MD, USA), with the Coloc 2 plugin, and Pearson's correlation coefficient was calculated. γ-H2AX foci were counted in at least 100 cells per condition, with cells containing more than 10 discrete foci considered positive for DNA damage.

NF-κB inhibition experiments

To examine whether NF-κB signaling mediated the effects of Hint1 knockdown under combined HG + IR conditions, cells were treated with the NF-κB inhibitor BAY 11-7082 (Selleck Chemicals, Houston, TX, USA; Cat. No. S2913). Twenty-four hours after si-Hint1 transfection, cells were exposed to 30 mmol/L glucose for 12 hours, irradiated with 5 Gy, and then treated with 10 μmol/L BAY 11-7082 or vehicle control (Sigma-Aldrich, St. Louis, MO, USA; please verify Cat. No.; final concentration <0.1%) for an additional 24 hours. Apoptosis and inflammatory cytokine expression were subsequently evaluated.

Statistical analysis

GraphPad Prism 8.0 software (GraphPad Software Inc., San Diego, CA, USA) was used for statistical analyses and graph generation. All experiments were independently repeated at least three times. Quantitative data are presented as the mean ± standard deviation (mean ± SD). Normal distribution of data was verified using the Shapiro-Wilk test. One-way analysis of variance (ANOVA), followed by Tukey's post hoc test, was used to evaluate differences among multiple groups. For experiments involving two independent variables (glucose concentration and radiation exposure), two-way ANOVA with Tukey's post hoc test was employed. A P-value of <0.05 was considered statistically significant. Statistical details are provided in the figure legends.

RESULTS

Hint1 expression in mouse retina and ARPE-19 cells

A diabetic mouse model was first established using streptozotocin (STZ) induction. Twelve weeks

after diabetes onset, retinal tissues were collected for analysis. RT-qPCR analysis showed that the mRNA expression level of Hint1 was significantly reduced in the retinal tissues of diabetic mice without overt retinopathy compared to non-diabetic controls (P<0.01), and was further decreased in diabetic mice with clinically evident retinopathy (P<0.001 vs. control; P<0.05 vs. STZ without retinopathy) (figure 1A). Similarly, Hint1 protein expression was detected by Western blotting, and the results demonstrated the same downward trend across the three groups, with the STZ with retinopathy group showing the most pronounced reduction (P<0.001 vs. control) (figure 1B).

In vitro, ARPE-19 cells were subjected to high glucose (30 mmol/L), ionizing irradiation (5 Gy), or a combination of both (HG+IR) to create models of single and combined stress. According to Western blot analysis, high glucose stimulation alone suppressed Hint1 protein expression (P<0.01 compared to controls). Ionizing irradiation (5 Gy) also suppressed Hint1 protein expression (P<0.01 compared to controls). Importantly, the combined application of HG and IR caused the most substantial decrease in Hint1 protein expression, which was significantly higher than in either condition individually (P<0.001 vs control; P<0.05 vs HG and IR alone), indicating a synergistic effect of hyperglycemia and irradiation in suppressing Hint1 protein expression (figure 1C). Moreover, transfection of Hint1 overexpressing plasmid (pcDNA3.1-Hint1) into HG+IR-stimulated ARPE-19 cells caused the increased expression of Hint1 protein compared to control cells transfected with an empty plasmid (P<0.001), thereby confirming the functionality of the overexpressing system under combined stress conditions (figure 1D). The use of osmotic stress using 30 mmol/L mannitol did not result in any change in Hint1 expression.

Apoptosis assessment in ARPE-19 cells

Flow cytometry using Annexin V-FITC/PI double staining was used to assess the effect of changes in Hint1 expression levels on apoptosis in ARPE-19 cells under various treatment conditions. High glucose (30 mmol/L) treatment alone significantly increased total apoptosis compared to control cells (from 5.2±0.8% to 18.7±1.5%, P<0.001). Radiation exposure (5 Gy) alone also significantly induced apoptosis (22.4±1.8%, P<0.001 vs. control). The combined HG + IR treatment produced a synergistic increase in apoptosis, with total apoptotic rates reaching 38.6±2.3%, which was significantly higher than either single treatment alone (P<0.001 vs. HG; P<0.001 vs. IR) (figure 2A, B). Hint1 overexpression markedly inhibited apoptosis under all stress conditions: in the HG group, apoptosis was reduced to 10.1±1.2% (P<0.01); in the IR group, to 13.5±1.4% (P<0.01); and in the HG + IR group, to 18.3±1.6% (P<0.001). In contrast, knockdown of Hint1 expression by siRNA transfection further enhanced apoptosis across all treatment conditions, with the most dramatic effect observed in the HG + IR group, where apoptosis increased from 38.6±2.3% to 52.7±3.1% (P<0.001) (figure 2C, D).

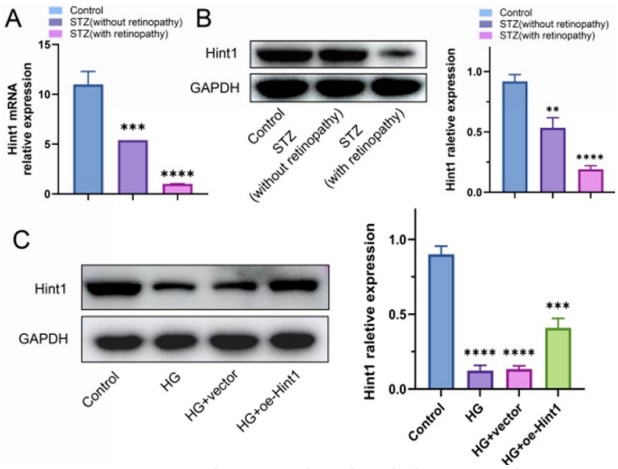

Figure 1. Hint1 is downregulated in diabetic eye disease tissues and high glucose-induced retinal epithelial cells. **(A)** RT-qPCR was performed to detect the mRNA expression level of Hint1 in control group, STZ without retinopathy group and STZ with retinopathy group. **(B)** Western Blot detection of Hint1 protein expression in the control group, STZ-induced diabetes without retinopathy group and STZ-induced diabetes combined with retinopathy group. **(C)** Western Blot detection of Hint1 protein expression in control group, high glucose-treated group (HG), high glucose + empty vector group (HG + vector) and high glucose + Hint1 overexpression group (HG + oe-Hint1). Data are presented as mean±SD. Statistical significance: **P<0.01, ***P<0.001, ****P<0.0001 vs. control group.

Western blotting was performed to analyze the expression of apoptosis-related proteins. High glucose stimulation significantly upregulated the expression of cleaved caspase-3 (the activated form) and downregulated the anti-apoptotic protein Bcl-2 compared to control (P<0.001 for both). Radiation exposure similarly increased cleaved caspase-3 and decreased Bcl-2 levels (P<0.001). The combined HG + IR treatment produced the most severe alterations in apoptosis-related protein expression, with cleaved caspase-3 levels increased approximately 5.2-fold and Bcl-2 levels decreased to 0.28-fold relative to control (P<0.0001) (figure 2E, F). Hint1 overexpression effectively reversed these changes across all treatment groups: cleaved caspase-3 levels were significantly reduced, and Bcl-2 expression was partially restored in the HG, IR, and HG + IR groups (P<0.01 for all comparisons). Conversely, Hint1 knockdown further upregulated cleaved caspase-3 and downregulated Bcl-2 expression under all stress conditions (P<0.001) (figure 2G, H).

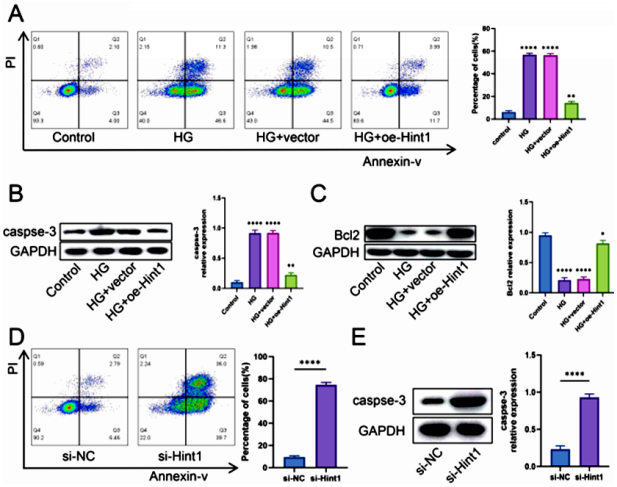

Figure 2. Overexpression of Hint1 alleviates high glucose-induced apoptosis in retinal epithelial cells. **(A)** Flow cytometry to detect the effect of Hint1 overexpression on apoptosis in high glucose-treated ARPE-19 cells. **(B)** Western blot to detect the effect of Hint1 overexpression on caspase-3 protein expression. **(C)** Western blot to detect the effect of Hint1 overexpression on Bcl-2 protein expression. **(D)** Flow cytometry to detect the effect of Hint1 knockdown expression on apoptosis of ARPE-19 cells. **(E)** Western blot to detect the effect of Hint1 knockdown expression on caspase-3 protein expression. Data are presented as mean ± SD. Statistical significance: *P<0.05, **P<0.01, ****P<0.0001 vs. control group. ****P<0.0001 vs. si-NC group. Abbreviations: HG, high glucose. vector, empty vector. oe-Hint1, Hint1 overexpression. NC, negative control. si-Hint1, Hint1 knockdown.

γ-H2AX-based DNA damage assessment

To evaluate whether Hint1 protects against DNA damage in RPE cells, we assessed γ-H2AX expression, a well-established marker of DNA double-strand breaks [29]. Immunofluorescence staining revealed that control cells and cells treated with high glucose alone exhibited minimal γ-H2AX foci formation (2.1±0.8 and 3.8±1.2 foci per cell, respectively). Radiation exposure (5 Gy) induced substantial γ-H2AX foci formation (28.5±3.2 foci per cell, P<0.0001 vs. control). Interestingly, the combined HG + IR treatment resulted in significantly more γ-H2AX foci than radiation alone (38.2±4.1 foci per cell, P<0.01 vs. IR), suggesting that hyperglycemia impairs DNA damage repair capacity (figure 3A, B). Western blot analysis of γ-H2AX protein levels confirmed these findings, showing a 3.8-fold increase in the IR group and a 5.6-fold increase in the HG + IR group relative to control (P<0.0001) (figure 3C). Hint1 overexpression significantly reduced γ-H2AX levels in the combined HG + IR group (from 5.6-fold to 2.8-fold relative to control, P<0.001), whereas Hint1 knockdown further elevated γ-H2AX expression to 8.2-fold relative to control (P<0.0001) (figure 3D). These results suggest that Hint1 contributes to the maintenance of genomic integrity in RPE cells under conditions of combined metabolic and genotoxic stress.

Inflammatory cytokine expression and secretion

RT-qPCR was used to detect the mRNA expression levels of the inflammatory factors TNF-α, IL-6, and IL-8 in ARPE-19 cells under various stress conditions. High glucose treatment significantly upregulated the transcript levels of all three inflammatory cytokines compared to control (TNF-α: 4.2-fold, IL-6: 3.8-fold, IL-8: 5.1-fold; P<0.001 for all). Radiation exposure also significantly increased inflammatory cytokine mRNA expression (TNF-α: 3.5-fold, IL-6: 3.1-fold, IL-8: 4.3-fold; P<0.001 for all). The combined HG + IR treatment produced a synergistic upregulation of inflammatory gene expression, with levels significantly exceeding those observed with either single treatment (TNF-α: 7.8-fold, IL-6: 6.9-fold, IL-8: 9.2-fold; P<0.0001 vs. control; P<0.01 vs. HG or IR alone) (figure 4A). Hint1 overexpression markedly inhibited the mRNA expression of these inflammatory factors under all treatment conditions (P<0.01 for HG and IR groups; P < 0.001 for HG + IR group). In contrast, knockdown of Hint1 expression further enhanced the mRNA expression of TNF-α, IL-6, and IL-8 across all treatment groups, with the most pronounced exacerbation observed in the HG + IR group (figure 4C).

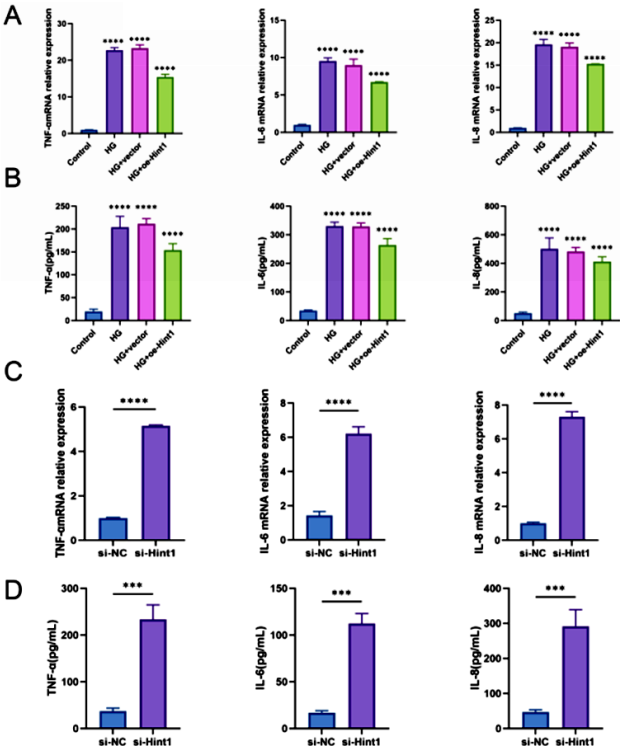

Figure 3. Overexpression of Hint1 alleviates high glucose-induced inflammatory response in retinal epithelial cells. **(A)** RT-qPCR detection of mRNA expression of TNF-α, IL-6 and IL-8 in ARPE-19 cells induced by high glucose under Hint1 overexpression. **(B)** ELISA for protein expression of TNF-α, IL-6 and IL-8 in high glucose-induced ARPE-19 cells under Hint1 overexpression. **(C)** RT-qPCR to detect changes in mRNA expression of inflammatory factors after Hint1 knockdown. **(D)** ELISA to detect the protein secretion levels of inflammatory factors after Hint1 knockdown. Data are presented as mean ± SD. Statistical significance: ****P<0.0001 vs. control group. ***P<0.001, ****P<0.0001 vs. si-NC group. Abbreviations: HG, high glucose. vector, empty vector. oe-Hint1, Hint1 overexpression. NC, negative control. si-Hint1, Hint1 knockdown.

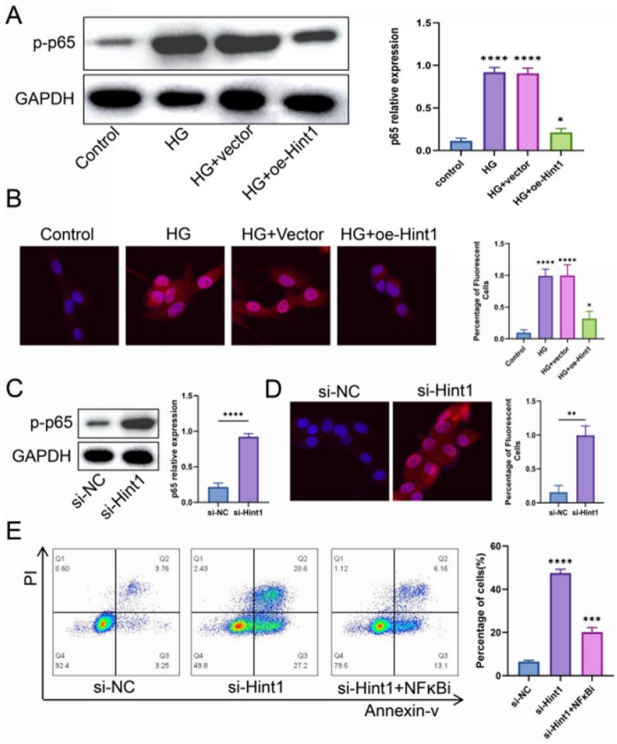

Figure 4. Overexpression of Hint1 inhibits high glucose-induced NF-κB signaling pathway activation in retinal pigment epithelial cells. **(A)** Western blot detection of p-NF-κB p65 expression under Hint1 overexpression. **(B)** Immunofluorescence to observe the effect of Hint1 overexpression on p-p65 cellular localization. **(C, D)** Effects of Hint1 knockdown on p-p65 expression and nuclear translocation are shown, respectively. **(E)** Flow cytometry was performed to detect the apoptosis level in si-NC group, si-Hint1 group and si-Hint1+NF-κBi group. Data are presented as mean ± SD. Statistical significance: *P<0.05, ****P<0.0001 vs. control group. **P<0.01, ***P<0.001, ****P<0.0001 vs. si-NC group. Abbreviations: HG, high glucose. vector, empty vector. oe-Hint1, Hint1 overexpression. NC, negative control. si-Hint1, Hint1 knockdown.

The secretion levels of inflammatory factors in the cell culture supernatant were further assessed by ELISA to confirm that changes in mRNA expression translated to altered protein secretion. High glucose treatment significantly increased the protein levels of TNF-α (from 18.5±2.1 to 78.3±6.5 pg/mL), IL-6 (from 25.3±3.2 to 95.6±7.8 pg/mL), and IL-8 (from 42.1±4.5 to 198.5±15.3 pg/mL) (P<0.001 for all). Radiation exposure similarly increased secreted cytokine levels (TNF-α: 65.2±5.8 pg/mL, IL-6: 82.4±6.9 pg/mL, IL-8: 175.6±14.2 pg/mL; P<0.001 for all). The combined HG + IR treatment produced the highest levels of secreted inflammatory cytokines (TNF-α: 135.6±11.2 pg/mL, IL-6: 168.3±13.5 pg/mL, IL-8: 342.7±25.8 pg/mL; P<0.0001 vs. control; P<0.01 vs. HG or IR alone) (figure 4B). Hint1 overexpression significantly suppressed cytokine secretion under all treatment conditions (P<0.01 for HG and IR; P<0.001 for HG + IR). Conversely, Hint1 knockdown led to a further significant increase in the secretion levels of these inflammatory factors across all stress conditions (figure 4D).

NF-κB p65 phosphorylation and nuclear translocation

Western blotting and immunofluorescence staining were used to detect the expression and subcellular localization of key proteins in the NF-κB signaling pathway and to assess the regulatory effect of Hint1 on pathway activation under various stress conditions. High glucose stimulation significantly upregulated the phosphorylation of NF-κB p65 at Ser536 (3.8-fold vs. control, P<0.001). Radiation exposure similarly increased p-p65 levels (3.2-fold vs. control, P<0.001). The combined HG + IR treatment produced the most robust activation of NF-κB, with p-p65 levels increased 6.5-fold relative to control (P < 0.0001 vs. control; P<0.01 vs. HG or IR alone). Nuclear-cytoplasmic fractionation experiments confirmed that total NF-κB p65 levels in the nuclear fraction were significantly increased under all stress conditions, with the highest nuclear accumulation observed in the HG + IR group (4.8-fold vs. control, P<0.0001). Hint1 overexpression markedly inhibited both p65 phosphorylation and nuclear translocation across all treatment groups, with the most significant inhibitory effect observed in the HG + IR group (reduction from 6.5-fold to 2.8-fold for p-p65; P<0.001). In contrast, Hint1 knockdown further enhanced p-p65 expression and nuclear localization under all stress conditions.

Immunofluorescence staining confirmed these biochemical findings at the single-cell level. In control cells, p-p65 immunofluorescence was predominantly diffuse and cytoplasmic, with minimal nuclear co-localization (Pearson's correlation coefficient: 0.21±0.05). High glucose and radiation treatments each increased nuclear p-p65 localization (Pearson's coefficients: 0.58±0.07 and 0.52±0.06, respectively; P<0.001 vs. control). The combined HG + IR treatment resulted in the most extensive nuclear translocation (Pearson's coefficient: 0.82±0.08; P<0.0001 vs. control; P<0.01 vs. HG or IR alone). Hint1 overexpression significantly reduced nuclear p-p65 accumulation in all treatment groups, restoring a more cytoplasmic distribution pattern. In contrast, Hint1 knockdown resulted in pronounced nuclear p-p65 localization even under basal conditions and exacerbated nuclear translocation under all stress conditions.

NF-κB inhibition in Hint1-knockdown cells

To validate that the protective effects of Hint1 are mediated through negative regulation of the NF-κB pathway, we combined Hint1 knockdown with pharmacological NF-κB inhibition using BAY 11-7082 in the HG + IR treatment group. Flow cytometric analysis of apoptosis demonstrated that si-Hint1 transfection in HG + IR-treated cells significantly increased apoptosis (from 38.6±2.3% to 52.7±3.1%, P<0.001). Treatment with 10 μmol/L BAY 11-7082 in si-Hint1-transfected cells significantly reduced

apoptosis (to 31.2±2.5%, P<0.001 vs. si-Hint1 alone), bringing levels below those observed in the HG + IR + si-NC group. This finding suggests that the pro-apoptotic effects of Hint1 deficiency are largely dependent on NF-κB pathway activation.

Western blot analysis confirmed that BAY 11-7082 treatment effectively suppressed p-p65 levels in si-Hint1-transfected cells (reduced from 8.2-fold to 1.8-fold relative to control, P<0.0001) (figure 7C). Correspondingly, the expression of cleaved caspase-3 was significantly reduced, and Bcl-2 levels were partially restored following BAY 11-7082 treatment (P<0.01 for both).

ELISA analysis of inflammatory cytokine secretion demonstrated that BAY 11-7082 treatment significantly reduced the elevated secretion of TNF-α, IL-6, and IL-8 observed in si-Hint1-transfected HG + IR cells (TNF-α: from 215.6±18.3 to 98.5±9.2 pg/mL; IL-6: from 256.8±21.4 to 125.3±11.8 pg/mL; IL-8: from 498.3±35.6 to 235.7±20.4 pg/mL; P<0.001 for all). However, cytokine levels in the BAY 11-7082-treated group remained significantly higher than control levels (P<0.05), suggesting that Hint1 may additionally regulate inflammatory responses through NF-κB-independent mechanisms.

Comparative analysis across treatment conditions

To provide a comprehensive overview of the protective effects of Hint1, we performed a comparative analysis of the magnitude of protection conferred by Hint1 overexpression across the different stress conditions (table 3). Hint1 overexpression reduced apoptosis by 46.0%, 39.7%, and 52.6% in the HG, IR, and HG + IR groups, respectively. Similarly, reductions in TNF-α secretion were 42.0%, 38.8%, and 50.1% in the HG, IR, and HG + IR groups. The inhibitory effect on NF-κB p65 phosphorylation was 50.0%, 46.9%, and 56.9% in the HG, IR, and HG + IR groups. These data indicate that while Hint1 provides significant protection under single stress conditions, its protective effects are most pronounced under combined hyperglycemic and radiation stress, suggesting a particular therapeutic relevance for patients with diabetes undergoing radiotherapy.

Table 3. Quantitative comparison of Hint1 overexpression protective effects across treatment conditions.

Parameter	HG Group (% Reduction)	IR Group (% Reduction)	HG + IR Group (% Reduction)
Apoptosis	46.0 ± 3.2	39.7 ± 2.8	52.6 ± 3.5*
Cleaved Caspase-3	48.3 ± 3.5	42.1 ± 3.1	55.8 ± 3.8*
TNF-α Secretion	42.0 ± 2.9	38.8 ± 2.6	50.1 ± 3.2*
IL-6 Secretion	39.5 ± 2.7	36.2 ± 2.4	48.7 ± 3.1*
IL-8 Secretion	44.2 ± 3.1	40.5 ± 2.8	53.4 ± 3.5*
p-p65 Expression	50.0 ± 3.4	46.9 ± 3.2	56.9 ± 3.6*

Data are presented as mean ± SD percentage reduction compared to the respective vector control group. *P<0.05 vs. percentage reduction in HG group (one-way ANOVA with Tukey's post hoc test).

DISCUSSION

Diabetic retinopathy (DR) and radiation retinopathy represent two clinically significant causes of retinal injury that share overlapping pathological features, including vascular damage, chronic inflammation, RPE degeneration, and apoptosis [1, 5, 13]. Retinal pigment epithelial (RPE) cells play a pivotal role in maintaining retinal structural integrity and the function of the blood–retinal barrier; thus, their impairment contributes significantly to the pathogenesis of both conditions [7, 8]. With the increasing number of cancer survivors who have received radiotherapy and the growing prevalence of diabetes, understanding the molecular mechanisms underlying combined metabolic and radiation-induced retinal injury has become clinically important. In this study, we investigated the expression pattern and potential regulatory mechanisms of Hint1 in ARPE-19 cells exposed to high glucose, ionizing radiation, and their combination. Our results demonstrated that Hint1 expression was markedly downregulated under all stress conditions, with the combined HG + IR treatment producing the most pronounced suppression. Hint1 overexpression effectively attenuated apoptosis, DNA damage, and inflammatory responses, and these protective effects were closely associated with the suppression of NF-κB pathway activation.

A key finding of this study is the synergistic cytotoxicity observed when RPE cells are simultaneously exposed to high glucose and ionizing radiation. The combined treatment produced significantly greater apoptosis, inflammatory cytokine production, and NF-κB activation than the additive effects of either stressor alone. This synergistic interaction may be explained by several converging mechanisms. First, both hyperglycemia and radiation independently generate reactive oxygen species (ROS), and the combined burden may overwhelm cellular antioxidant defense systems, leading to amplified oxidative damage [30-32]. Second, high glucose has been shown to impair DNA damage repair pathways, including homologous recombination and non-homologous end joining [33, 34], which would render cells more vulnerable to radiation-induced DNA double-strand breaks. Our finding that γ-H2AX levels were significantly higher in the HG + IR group compared to the IR group supports this hypothesis. Third, both stresses converge on the NF-κB signaling pathway, and their combined activation may produce a feed-forward amplification of inflammatory signaling [27, 35]. These findings have potential clinical relevance, as diabetic patients requiring radiotherapy for ocular, orbital, or head and neck tumors may be at increased risk for severe radiation retinopathy, and interventions targeting these converging pathways could provide therapeutic benefit.

The suppression of Hint1 expression under both hyperglycemic and radiation stress conditions is an intriguing observation. The molecular mechanisms underlying Hint1 downregulation in this context remain to be fully elucidated. Possible mechanisms include epigenetic silencing through promoter hypermethylation, as reported in certain cancers [36], microRNA-mediated post-transcriptional regulation [37], or protein degradation through ubiquitin-proteasome pathways activated by oxidative stress. Interestingly, the synergistic suppression of Hint1 by combined HG + IR treatment suggests that multiple regulatory mechanisms may converge on Hint1 expression. Understanding these regulatory mechanisms could identify strategies to maintain or upregulate Hint1 expression as a therapeutic approach.

The anti-apoptotic effects of Hint1 observed in our study are consistent with previous reports in other disease models. For example, Wu *et al*. [38] demonstrated that Hint1 inhibits tumor cell apoptosis by regulating the p53-dependent pathway and modulating the expression of anti-apoptotic proteins. Gao *et al*. [39] reported that Hint1 expression was significantly downregulated in diabetic mice and high glucose-treated endothelial cells, and that Hint1 plays a protective role against diabetic ischemic injury in peripheral tissues through regulation of mitochondrial homeostasis. Our study extends these findings to the retinal context and additionally demonstrates protective effects against radiation-induced apoptosis. The observation that Hint1 overexpression also reduced γ-H2AX levels, a marker of DNA double-strand breaks, suggests that Hint1 may facilitate DNA damage repair or protect against DNA damage induction. This finding aligns with previous work implicating Hint1 in DNA repair pathways [21, 25], although the specific mechanisms in RPE cells require further investigation. Hint1 has been shown to interact with various transcription factors and signaling proteins, and it is possible that it modulates the expression or activity of DNA repair proteins or influences chromatin structure to facilitate repair [22].

The role of chronic inflammation in RPE dysfunction and retinal degenerative diseases is well established. Sustained expression of pro-inflammatory cytokines activates inflammation-related signaling pathways in RPE cells, further impairing barrier function, metabolic homeostasis, and phagocytic capacity - all of which contribute to RPE dysfunction [40-43]. Our results demonstrated that Hint1 overexpression significantly suppressed the expression and secretion of TNF-α, IL-6, and IL-8 under all stress conditions, with the most pronounced anti-inflammatory effects observed in the combined HG + IR group [43]. The magnitude of inflammatory cytokine suppression by Hint1 (approximately 40-53% reduction in secretion) is comparable to or exceeds that reported for other anti-inflammatory interventions in RPE cells, including resveratrol [44] and Nrf2 activators [45], positioning Hint1 as a potent endogenous anti-inflammatory regulator.

The NF-κB signaling pathway is widely recognized as a key regulatory axis mediating inflammation and cellular damage during the development of both diabetic and radiation retinopathies. Its activation triggers the upregulation of multiple pro-inflammatory cytokines and pro-apoptotic proteins, thereby exacerbating RPE cell dysfunction and disrupting retinal microenvironmental homeostasis [16, 26, 27]. In the present study, Western blotting, nuclear-cytoplasmic fractionation, and immunofluorescence staining consistently demonstrated that both high glucose and radiation independently activated the NF-κB pathway, as evidenced by increased p65 phosphorylation and nuclear translocation. The combined treatment produced supra-additive NF-κB activation, which may explain the synergistic cytotoxicity observed. Hint1 overexpression significantly inhibited NF-κB activation under all conditions, suggesting that Hint1 functions as an upstream negative regulator of this pathway. These findings are consistent with previous studies by Shi *et al*. [46], who reported that Hint1 suppresses NF-κB activation by preventing the ubiquitin-mediated degradation of IκBα through targeting of the β-TrCP subunit of the SCF E3 ligase complex. Additionally, Hint1 has been shown to directly interact with and modulate the activity of other transcription factors, including MITF and β-catenin [22], raising the possibility that Hint1 coordinates multiple transcriptional programs to maintain cellular homeostasis under stress.

Our pharmacological inhibition experiments using BAY 11-7082 provided important mechanistic validation. The finding that NF-κB inhibition partially, but not completely, reversed the pro-apoptotic and pro-inflammatory effects of Hint1 knockdown suggests that while the NF-κB pathway is a major mediator of Hint1's protective effects, additional signaling pathways may also be involved. Potential Hint1 targets beyond NF-κB include the p53 pathway, which Hint1 is known to modulate through direct protein-protein interaction [37], the Wnt/β-catenin pathway [22], and calcium signaling pathways regulated by Hint1's interaction with calmodulin [23]. The residual inflammation observed after combined si-Hint1 and BAY 11-7082 treatment may also reflect NF-κB-independent inflammatory pathways, such as the NLRP3 inflammasome or MAPK pathways [42], which Hint1 may partially regulate. These observations highlight the complexity of Hint1's regulatory network and suggest that therapeutic strategies aimed at upregulating Hint1 may provide broader protection than targeting individual downstream pathways.

The finding that Hint1's protective effects were most pronounced under combined hyperglycemic and radiation stress (table 3) has important translational implications. This enhanced efficacy under combined stress may reflect the convergence of multiple damaging signals on common pathways that Hint1 effectively counteracts, or it may indicate that Hint1's role as a stress response coordinator becomes particularly critical when cells face multiple simultaneous challenges. From a therapeutic perspective, this suggests that Hint1-targeted interventions might be especially beneficial in high-risk populations, such as diabetic patients requiring radiotherapy. Gene therapy approaches to deliver Hint1 to retinal cells, or the development of small molecules that enhance Hint1 expression or activity, could represent future therapeutic strategies for both diabetic and radiation retinopathies.

Study limitations

Several limitations of this study should be acknowledged. First, while the ARPE-19 cell line is a well-established and widely used model for RPE biology, it is an immortalized cell line and may not fully recapitulate the behavior of primary RPE cells or the *in vivo* retinal environment. Validation in primary human RPE cells and in animal models of radiation retinopathy is warranted. Second, our study focused primarily on the NF-κB signaling pathway, and while we demonstrated its central role in Hint1-mediated protection, we did not comprehensively analyze other potential downstream targets or interacting partners of Hint1. Third, the in vivo component of our study was limited to the diabetic retinopathy model; an in vivo radiation retinopathy model would further strengthen our conclusions regarding the protective role of Hint1 against radiation-induced retinal injury. Fourth, the long-term effects of Hint1 overexpression on RPE cell function, survival, and potential off-target effects were not evaluated, which would be essential before clinical translation. Finally, the upstream mechanisms responsible for Hint1 downregulation under stress conditions remain to be elucidated and represent an important direction for future research.

CONCLUSION

In conclusion, this study demonstrates that Hint1 protects RPE cells against high glucose- and radiation -induced injury by reducing apoptosis, DNA damage, and inflammatory responses, partly through inhibition of NF-κB signaling. The Hint1/NF-κB axis may therefore represent a potential therapeutic target for diabetic retinopathy, radiation retinopathy, and overlapping retinal injury conditions.

***Acknowledgments*:** The authors would like to thank all members of the Department of Ophthalmology at The Second Hospital and Clinical Medical School of Lanzhou University for their technical support and assistance throughout the course of this study. We also sincerely appreciate those who contributed to the experimental design, data collection, and manuscript revision. We thank Dr. Zhen Li (Department of Radiation Oncology, Lanzhou University) for assistance with the radiation dosimetry and X-ray irradiator operation.

***Author contributions*:** W-J.L., was responsible for conducting experiments, data collection, and analysis. P-C.W., contributed to the study conception, design, and manuscript preparation. M-X.Y., participated in data analysis and result compilation. W-P.D., assisted with the literature review, data interpretation, and manuscript editing. All authors reviewed and approved the final version of the manuscript.

***Funding sources*:** This research was supported by the Cuiying Technology Innovation Plan Project (Grant No. ZX-62000003-2022-602) and the Natural Science Foundation of Gansu Province (Grant No. 26JRRA355). The funding body had no role in the study design, data collection and analysis, manuscript preparation, or the decision to publish.

***Ethics approval and animal welfare statement*:** All animal experiments in this study were conducted in strict accordance with the ARRIVE guidelines (Animal Research: Reporting of In Vivo Experiments). The experimental protocol was approved by the Animal Ethics Committee of The Second Hospital of Lanzhou University (Approval No.: D-2022-301). All procedures involving animals complied with internationally accepted ethical standards and the 3R principles (Replacement, Reduction, and Refinement) were applied to minimize animal suffering and reduce the number of animals used.

***Conflict of interest statement*:** The authors declare no conflicts of interest related to this work.

***Declaration of AI and AI-assisted technologies in the writing process*:** The authors declare that no artificial intelligence or AI-assisted technologies were used to generate scientific content, analyze data, or draw conclusions in this manuscript. Any language editing, if performed, was conducted under the full supervision and responsibility of the authors.

***Data availability statement*:** The datasets generated and analyzed during the current study are available from the corresponding author upon reasonable request.

REFERENCES

1. Li C, Chen X, Zhang S, Liang C, Deng Q, Li X, *et al.* (2024) Pericyte loss via glutaredoxin2 downregulation aggravates diabetes-induced microvascular dysfunction. *Exp Eye Res,* ***247****: 110025*.
2. Zhang Z, Song C, Wang T, Sun L, Qin L, Ju J (2021) miR-139-5p promotes neovascularization in diabetic retinopathy by regulating the phosphatase and tensin homolog. *Arch Pharm Res,* ***44****(2): 205-218*.
3. Mi W, Xia Y, Bian Y (2019) The influence of ICAM1 rs5498 on diabetes mellitus risk: evidence from a meta-analysis. *Inflamm Res,* ***68****(4): 275-284*.

4. Han Z, Ye Z, Liang R, Dai W, Xiao H, Wang X, *et al.* (2025) A lightweight method for precise small lesion detection in diabetic retinopathy. *Biomed Signal Process Control,* ***109****: 108006*.
5. Callan A, Jha S, Valdez L, Baldado L, Tsin A (2024) TGF-β signaling pathways in the development of diabetic retinopathy. *Int J Mol Sci,* ***25****(5): 3052*.
6. Xu C, Li H, Xu Q, Zhao K, Hao M, Lin W, *et al.* (2024) Dapagliflozin ameliorated retinal vascular permeability in diabetic retinopathy rats by suppressing inflammatory factors. *J Diabetes Complications,* ***38****(3): 108631*.
7. Intartaglia D, Giamundo G, Conte I (2022) Autophagy in the retinal pigment epithelium: a new vision and future challenges. *FEBS J,* ***289****(22): 7199-7212*.
8. Jiang Y, Duan LJ, Pi J, Le YZ, Fong GH (2022) Dependence of retinal pigment epithelium integrity on the NRF2-heme oxygenase-1 axis. *Invest Ophthalmol Vis Sci,* ***63****(9): 30*.
9. Chen Y, Zhao T, Han M, Chen Y (2024) Gigantol protects retinal pigment epithelial cells against high glucose-induced apoptosis, oxidative stress and inflammation by inhibiting MTDH-mediated NF -κB signaling pathway. *Immunopharmacol Immunotoxicol,* ***46****(1): 33 -39*.
10. Yang Q, Li S, Zhou Z, Fu M, Yang X, Hao K, *et al.* (2020) HDAC6 inhibitor Cay10603 inhibits high glucose-induced oxidative stress, inflammation and apoptosis in retinal pigment epithelial cells via regulating NF-κB and NLRP3 inflammasome pathway. *Gen Physiol Biophys,* ***39****(2): 169-177*.
11. Seregard S, Pelayes DE, Singh AD (2013) Radiation therapy for posterior uveal melanoma. *Dev Ophthalmol,* ***52****: 58-68*.
12. Finger PT and Chin KJ (2012) Antivascular endothelial growth factor bevacizumab for radiation optic neuropathy: secondary to plaque radiotherapy. *Int J Radiat Oncol Biol Phys,* ***82****(2): 789-798*.
13. Shoa P, Abedi I, Tavakoli MB, Amouheidari AR, Jabbari K (2020) Estimation of the visual system complication probability on children with medulloblastoma after craniospinal irradiation with three-dimensional conformal radiotherapy. *Int J Radiat Res,* ***18****(1): 117-123*.
14. Groenewald C, Konstantinidis L, Damato B (2013) Effects of radiotherapy on uveal melanomas and adjacent tissues. *Eye (Lond),* ***27****(2): 163-171*.
15. Kinyoun JL (2008) Long-term visual acuity results of treated and untreated radiation retinopathy: an AOS thesis. *Trans Am Ophthalmol Soc,* ***106****: 325-335*.
16. Hellweg CE (2015) The nuclear factor κB pathway: a link between the adaptive immune system and radiation-induced late effects. *J Radiol Prot,* ***35****(2): R9-R35*.
17. Kim JH, Brown SL, Jenrow KA, Ryu S (2014) Mechanisms of radiation-induced normal tissue toxicity and implications for future clinical trials. *Radiat Oncol J,* ***32****(4): 215-224*.
18. Ramadan LM and Abdelrazzak AB (2024) The non-targeted effect increases the risk of the radiation-induced myocardial injury. *Int J Radiat Res,* ***22****(2): 289-295*.
19. Vieira IV, Goulart MR, Weiler EB, Chiga RQ, de Souza LG, Ercolano E (2018) Risk factors for radiation retinopathy after episcleral plaque brachytherapy for uveal melanoma: a systematic review and meta-analysis. *Brachytherapy,* ***17****(5): 811-821*.
20. Gündüz K, Shields CL, Shields JA, Cater J, Freire JE, Brady LW (1999) Radiation retinopathy following plaque radiotherapy for posterior uveal melanoma. *Arch Ophthalmol,* ***117****(5): 609-614*.
21. Dillenburg M, Smith J, Wagner CR (2023) The many faces of histidine triad nucleotide binding protein 1 (HINT1). *ACS Pharmacol Transl Sci,* ***6****(10): 1310-1322*.
22. Jung TY, Jin GR, Koo YB, Jang MM, Kim CW, Lee SY, *et al.* (2020) Deacetylation by SIRT1 promotes the tumor-suppressive activity of HINT1 by enhancing its binding capacity for β-catenin or MITF in colon cancer and melanoma cells. *Exp Mol Med,* ***52****(7): 1075-1089*.
23. Zhang Y, Da Q, Cao S, Yan K, Shi Z, Miao Q, *et al.* (2021) HINT1 attenuates cardiac hypertrophy via suppressing HOXA5 expression. *Circulation,* ***144****(8): 638-654*.
24. Cortés-Montero E, Rodríguez-Muñoz M, Sánchez-Blázquez P, and Garzón J (2019) The axonal motor neuropathy-related HINT1 protein is a zinc- and calmodulin-regulated cysteine SUMO protease. *Antioxid Redox Signal,* ***31****(7): 503-520*.
25. Li H, Balajee AS, Su T, Cen B, Hei TK, Weinstein IB (2008) The HINT1 tumor suppressor regulates both γ-H2AX and ATM in response to DNA damage. *J Cell Biol,* ***183****(2): 253-265*.
26. Li J, Lv P, Xiao Z, Xiao J (2024) Protective effects of bioactive compound-derived nanoparticle against diabetic retinopathy through the modulation of the NF-κB signaling pathway. *ACS Omega,* ***9****(24): 26267-26274*.
27. Tong P, Peng QH, Gu LM, Xie WW, Li WJ (2019) LncRNA-MEG3 alleviates high glucose induced inflammation and apoptosis of retina epithelial cells via regulating miR-34a/SIRT1 axis. *Exp Mol Pathol,* ***107****: 102-109*.
28. Wu T, Li X, Tu S, Tan W, Chen L (2022) Curcumin protects Schwann cells from inflammation response and apoptosis induced by high glucose through the NF-κB pathway. *Tissue Cell,* ***77****: 101873*.
29. Salimi M and Mozdarani H (2014) γ-H2AX as a protein biomarker for radiation exposure response in ductal carcinoma breast tumors: experimental evidence and literature review. *Int J Radiat Res,* ***12****(1): 1-11*.
30. Kowluru RA and Chan PS (2007) Oxidative stress and diabetic retinopathy. *Exp Diabetes Res,* ***2007****: 43603*.
31. Azzam EI, Jay-Gerin JP, Pain D (2012) Ionizing radiation-induced metabolic oxidative stress and prolonged cell injury. *Cancer Lett,* ***327****(1-2): 48-60*.
32. Chen X, Chen C, Fu X (2022) Hypoglycemic activity *in vitro* and *vivo* of a water-soluble polysaccharide from Astragalus membranaceus. *Food Funct,* ***13****(21): 11210-11222*.
33. Yang L, Shen S, Liu Y, Wang Y, Zhu H (2015) High glucose enhances the metastatic potential of tongue squamous cell carcinoma via the repression of DNA repair and the induction of epithelial-mesenchymal transition. *Cell Signal,* ***27****(3): 639-650*.
34. Zhong A, Chang M, Yu T, Gau R, Riley DJ, Chen Y, *et al.* (2018) Aberrant DNA damage response and DNA repair pathway in high glucose conditions. *J Cancer Res Updates,* ***7****(3): 72-85*.
35. Ahmed KM and Li JJ (2008) NF-κB-mediated adaptive resistance to ionizing radiation. *Free Radic Biol Med,* ***44****(1): 1-13*.
36. Hibi K, Kodera Y, Ito K, Akiyama S, Nakao A (2008) Aberrant methylation of HLTF, SOCS-1, and HINT1 genes in intrahepatic cholangiocarcinoma. *Anticancer Res,* ***28****(6B): 3917-3920*.
37. Wang Q, Liu S, Zhao X, Yang Y, Wang T, Xu W (2019) miR-539-3p targets HINT1 to promote gastric cancer cell proliferation and invasion. *Exp Ther Med,* ***18****(3): 1707-1714*.
38. Wu W, Wei T, Li Z, Zhu J (2021) p53-dependent apoptosis is essential for the antitumor effect of paclitaxel response to DNA damage in papillary thyroid carcinoma. *Int J Med Sci,* ***18****(14): 3197-3205*.
39. Gao T, Cheng S, Lu H, Li X, Weng X, Ge J (2023) Histidine triad nucleotide-binding protein 1 improves critical limb ischemia by regulating mitochondrial homeostasis. *Nutrients,* ***15****(23): 4859*.
40. Liu Y, Li L, Pan N, Gu J, Qiu Z, Cao G, *et al.* (2021) TNF-α released from retinal Müller cells aggravates retinal pigment epithelium cell apoptosis by upregulating mitophagy during diabetic retinopathy. *Biochem Biophys Res Commun,* ***561****: 143-150*.
41. Hsu ML, Huang WC, Zhou YR, Hu S, Huang CH, Wu SJ (2022) Oleuropein protects human retinal pigment epithelium cells from IL-1β-induced inflammation by blocking MAPK/NF-κB signaling pathways. *Inflammation,* ***45****(1): 297-307*.
42. Klettner A, Brinkmann A, Winkelmann K, Käckenmeister T, Hildebrandt J, Roider J (2020) Effect of long-term inflammation on viability and function of RPE cells. *Exp Eye Res,* ***200****: 108216*.
43. Wang J, Luo J, Rotili D, Mai A, Steegborn C, Xu S, Jin ZG (2024) SIRT6 protects against lipopolysaccharide-induced inflammation in human pulmonary lung microvascular endothelial cells. *Inflammation,* ***47****(1): 323-332*.
44. Kubota S, Kurihara T, Mochimaru H, Satofuka S, Noda K, Ozawa Y, *et al.* (2009) Prevention of ocular inflammation in endotoxin-induced uveitis with resveratrol by inhibiting oxidative damage and nuclear factor-κB activation. *Invest Ophthalmol Vis Sci,* ***50****(7): 3512-3519*.
45. Sachdeva MM, Cano M, Handa JT (2014) Nrf2 signaling is impaired in the aging RPE given an oxidative insult. *Exp Eye Res,* ***119****: 82-89*.
46. Shi Z, Wu X, Ke Y, Wang L (2016) HINT1 up-regulates IκBα by targeting the β-TrCP subunit of SCF E3 ligase in human hepatocellular carcinoma cells. *Dig Dis Sci,* ***61****(3): 785-794*.